Japanese Journal of Applied Physics

The Japan Society of Applied Physics

Vertical alignment control of self-ordered multilayered Ge nanodots on SiGe

OPEN ACCESS

Japanese Journal of Applied Physics **62**, SC1057 (2023) **REGULAR PAPER**

https://doi.org/**10.35848/1347-4065/acb05e**

Vertical alignment control of self-ordered multilayered Ge nanodots on SiGe

Wei-Chen Wen[1*], Markus Andreas Schubert[1], Bernd Tillack[1,2], and Yuji Yamamoto[1]

[1]*IHP - Leibniz-Institut für innovative Mikroelektronik, Im Technologiepark 25, 15236, Frankfurt (Oder), Germany*
[2]*Technische Universität Berlin, HFT4, Einsteinufer 25, 10587, Berlin, Germany*

[*]E-mail: wei-chen.wen@ihp-microelectronics.com

Received October 20, 2022; revised December 9, 2022; accepted January 4, 2023; published online February 7, 2023

Self-ordered multilayered Ge nanodots with SiGe spacers on a $Si_{0.4}Ge_{0.6}$ virtual substrate are fabricated using reduced-pressure chemical vapor deposition, and the mechanism of vertical ordering is investigated. The process conditions of Ge and SiGe layer deposition are H_2-GeH_4 at 550 °C and H_2-SiH_4-GeH_4 at 500 °C–550 °C, respectively. By depositing the SiGe at 550 °C or increasing Ge content, the SiGe surface becomes smooth, resulting in vertically aligned Ge nanodots to reduce strain energy. Ge nanodots prefer to grow on the nanodot where the SiGe is relatively tensile strained due to the buried Ge nanodot underneath. By depositing at 500 °C and lowering Ge content, checkerboard-like surface forms, and the following Ge nanodots grow at staggered positions to reduce surface energy. The Ge nanodots are laterally aligned along the elastically soft ⟨100⟩ direction without pre-structuring resulting from the strain distribution. © 2023 The Japan Society of Applied Physics

1. Introduction

To handle the ongoing exponential expansion of information, advanced technologies with improved electronic device performance are required. However, device performance using conventional existing group IV materials systems such as Si, SiGe and Ge have certain limitations because of their material properties. In order to overcome the limitation of the material properties, a potential breakthrough could be to develop novel artificial group IV materials such as superlattices (SL) and nanodots. Using a heteroepitaxial SL structure, a band gap and band offset can be engineered and novel material properties can be designed.[1,2)] Additionally, by fabricating a nanodot structure, it is possible to change the density of states in the conduction band and valence band.[3,4)] Therefore, three-dimensionally (3D) stacked SiGe and Ge nanodots of SL are of interest because of their potential for designing new optoelectrical material properties.

Multilayer Ge nanodots are of great interest due to the possibility of integration with the current complementary metal–oxide–semiconductor (CMOS) platform and the potential application for thermoelectric devices,[5)] tunneling diodes[6)] and optoelectronics, such as lasers[7–10)] and photodetectors.[11–13)] Many groups have studied self-assembled Ge nanodots grown by random nucleation according to the Stranski–Krastanov (SK) mechanism.[14–18)] To control the lateral alignment of Ge nanodots, pre-structuring is usually necessary. For the SiGe nanodot formation we have presented vertically and laterally ordered multi-layered SiGe nanodots in Si by SiGe/Si SL deposition without pre-structuring.[19,20)] By selecting SiH_4 or SiH_2Cl_2 as a precursor for the Si spacer growth, the surface morphology can be controlled. By proactively using local tensile strain and surface energy of the Si spacer surface, it is possible to control the following SiGe nanodot formation at on-dot positions or at staggered positions. For the Ge nanodot formation, we have reported dot-on-dot vertically and laterally aligned multilayered Ge nanodots with a Si spacer on SiGe nanodot SL as a template[21)] and with a SiGe spacer on a SiGe virtual substrate (VS) without pre-structuring.[22)]

In this study, we fabricated 3D self-ordered multilayered Ge nanodots on a SiGe VS with SiGe spacers. We also studied the influence of SiGe spacer growth conditions on the surface morphology and on Ge nanodot formation on these surfaces, which is the key to the vertical alignment control. Compared to the results published in Ref. 23 more in-depth discussions about the SiGe spacer formation and driving force for lateral alignment are given in this paper.

2. Experimental

The 3D self-ordered Ge nanodots were fabricated by reduced-pressure chemical vapor deposition (RPCVD). First, a $Si_{0.4}Ge_{0.6}$ VS with a step-graded buffer deposited on a Si (001) wafer was prepared using a H_2–SiH_4–GeH_4 gas mixture. To fabricate the high crystallinity $Si_{0.4}Ge_{0.6}$ VS, 500 nm thick SiGe layers with Ge content of 10%–50% with a 10% step, followed by 2 μm thick $Si_{0.4}Ge_{0.6}$, were deposited.[24–26)] In order to further improve the crystal quality of the VS, annealing at 1000 °C was performed after each step and after the whole layer deposition.[27–29)] A threading dislocation density of $\sim 1 \times 10^7\,cm^{-2}$ for the VS was achieved by this method. Furthermore, approximately 300 nm material was removed by chemical mechanical polishing to planarize the cross-hatch structure on the surface. A root mean square roughness of 0.3 nm was confirmed by atomic force microscopy (AFM).

After HF dip, the VS was loaded into the RPCVD reactor and baked at 850 °C in H_2 to remove residual native oxide. For SiGe and Ge deposition, H_2–SiH_4–GeH_4 and H_2–GeH_4 gas mixtures were used, respectively. To discuss the influence of SiGe growth condition on the surface morphology of the SiGe on Ge nanodots, a laterally ordered Ge nanodot structure of ~26 nm height and ~140 nm periodicity along ⟨100⟩ was prepared as a template. The template was fabricated by 20 cyclic depositions of 52 nm $Si_{0.48}Ge_{0.52}$ and 12.5 nm Ge SL on $Si_{0.4}Ge_{0.6}$ VS at 550 °C.[22)] On the template, a layer of 45–63 nm SiGe with Ge content of 45%–52% was deposited at 550 °C or 500 °C without air exposure.

To investigate the controllability of vertical alignment and positioning of the Ge nanodots, 20-cycle 52 nm

SiGe/12.5 nm Ge SL were directly deposited on the $Si_{0.4}Ge_{0.6}$ VS. For this SL, $Si_{0.48}Ge_{0.52}$ grown at 550 °C and $Si_{0.51}Ge_{0.49}$ or $Si_{0.48}Ge_{0.52}$ grown at 500 °C were alternately used as spacers.

In order to investigate the SiGe spacer growth behavior of the $Si_{0.48}Ge_{0.52}$ grown at 550 °C and the $Si_{0.51}Ge_{0.49}$ grown at 500 °C, 1–1.5 nm thick Ge marker layers were introduced in the SiGe spacers, by switching the SiH_4 flow to the vent line without changing temperature or GeH_4 flow for the selected samples.

AFM was used to analyze the SiGe surface morphology and lateral alignment of Ge nanodots, and scanning electron microscopy (SEM) was used to observe the vertical and lateral alignment of the Ge nanodots. Scanning transmission electron microscopy (STEM) and energy dispersive X-ray spectroscopy (EDX) were used to inspect the SiGe growth and the Ge content variation.

3. Results and discussion

Figures 1(a)–1(d) show the AFM images of 52 nm SiGe with Ge content of 45%–52% deposited at 550 °C or 500 °C on the laterally ordered Ge nanodot templates. The $Si_{0.51}Ge_{0.49}$ grown at 550 °C [Fig. 1(a)] shows a smooth surface while the one grown at 500 °C [Fig. 1(c)] shows a checkerboard-like surface. This checkerboard mesa structure formation is due to the insufficient surface migration of Si and/or Ge atoms to fill the space between Ge nanodots to form a smooth surface at 500 °C. Moreover, the checkerboard mesas become clearer with decreasing Ge content [Fig. 1(b)], while they become less clear and imperfect with increasing Ge content [Fig. 1(d)]. This trend may result from the increased ratio of adsorbed Ge atoms, which have lower binding energy and more surface migration compared to Si atoms during epitaxy. Thus, migrating to positions between Ge nanodots to reduce surface energy is more pronounced when Ge content is high.

The SiGe thickness and Ge content dependence of mesa width and height are summarized in Fig. 2. The mesa height increases with decreasing Ge content. At the same Ge concentration, the mesa height is not clearly influenced by the SiGe spacer thickness. This is due to more surface migration of Ge atoms compared to Si atoms as mentioned before. On the other hand, the mesa width increases with decreasing Ge concentration as well as thickness of the SiGe spacer. This means the SiGe growth is not only on the (001) surface but also on the mesa sidewall facet. With increasing SiGe thickness from 52 nm to 62 nm, the mesa width is increased by 3.5% for $Si_{0.48}Ge_{0.52}$. This increase in the mesa width becomes ~4.9% and 6.1% by changing the Ge concentration to 49% and 45%, respectively. The ratio of the growth rate on the sidewall facet to that on the (001) surface is higher at lower Ge content. This can also be explained by the higher surface migration of Ge atoms compared to Si atoms.

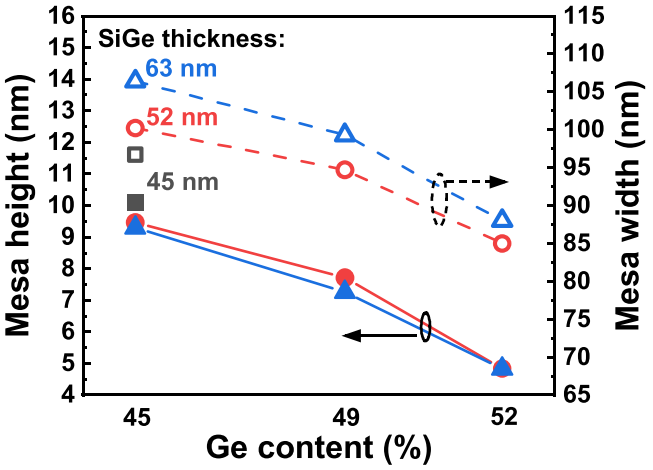

Fig. 2. (Color online) SiGe thickness dependence (45 nm, 52 nm and 63 nm) and Ge content dependence (45%, 49% and 52%) of mesa height (solid symbols) and width (open symbols). The SiGe layers were deposited on the laterally ordered Ge nanodot templates at 500 °C.

The influence of different SiGe surface morphology on Ge nanodot alignment can be seen from the cross-section SEM images as shown in Figs. 3(a)–3(b). The SiGe thickness and Ge thickness of the 20-cycle SL are 52 nm SiGe and 12.5 nm Ge, respectively, and for the SiGe spacer deposition, $Si_{0.48}Ge_{0.52}$ grown at 550 °C and $Si_{0.51}Ge_{0.49}$ [Fig. 3(a)] or $Si_{0.48}Ge_{0.52}$ grown at 500 °C [Fig. 3(b)] are deposited. In Fig. 3(a), the Ge nanodots on $Si_{0.48}Ge_{0.52}$ fabricated at 550 °C tend to grow on the buried nanodots. The vertical alignment of the dot-on-dot structure is due to locally higher lateral tensile strain arising from the buried Ge nanodot.[17,19] However, Ge nanodots grow at the staggered position on the $Si_{0.51}Ge_{0.49}$ fabricated at 500 °C. The surface morphology of the $Si_{0.51}Ge_{0.49}$ surface grown at 500 °C is checkerboard structured as shown in Fig. 1(c), and the Ge nanodot is deposited at the concave region between two mesas. The driving force seems to be the reduction of the surface energy caused by surface roughness.[19] The incompletely staggered growth on $Si_{0.48}Ge_{0.52}$ grown at 500 °C [Fig. 3(b)] is due to the insufficient checkerboard feature [Fig. 1(d)].

Next, the lateral alignment of Ge nanodots is discussed. The lateral alignment of Ge nanodots is inspected as shown in Fig. 4. The Ge nanodots are well ordered along the ⟨100⟩

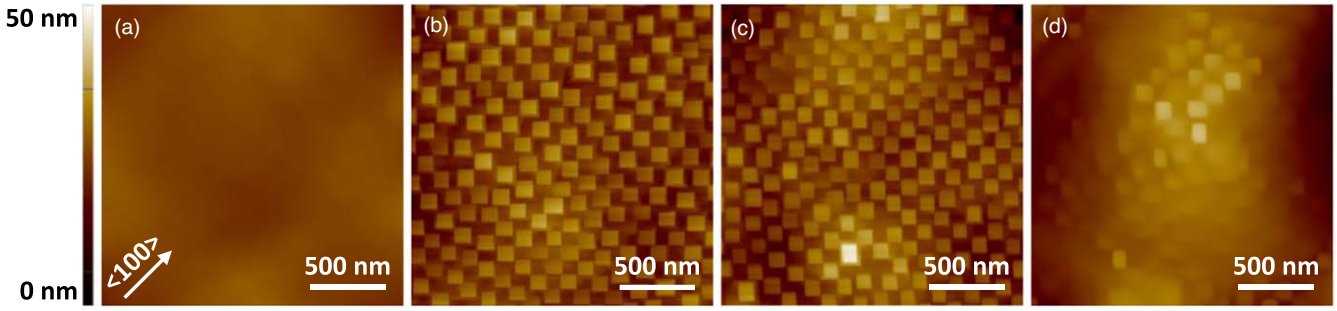

Fig. 1. (Color online) AFM images of 52 nm (a) $Si_{0.51}Ge_{0.49}$ grown at 550 °C, (b) $Si_{0.55}Ge_{0.45}$, (c) $Si_{0.51}Ge_{0.49}$ and (d) $Si_{0.48}Ge_{0.52}$ grown at 500 °C on laterally ordered Ge nanodot templates.

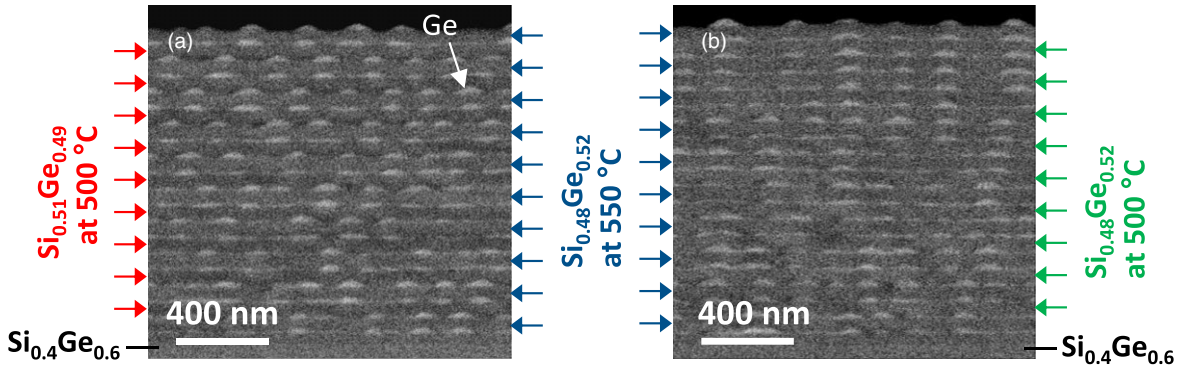

Fig. 3. (Color online) Cross section SEM images of 20-cycle SL of 52 nm SiGe/12.5 nm Ge. $Si_{0.48}Ge_{0.52}$ grown at 550 °C and (a) $Si_{0.51}Ge_{0.49}$ or (b) $Si_{0.48}Ge_{0.52}$ grown at 500 °C alternately used as spacers.

direction with a periodicity of approximately 145 nm [Fig. 4(a)], which is comparable to the dot-on-dot aligned Ge nanodots.[22] This lateral alignment is confirmed in the Fourier transform (FT) image of a 10 μm × 10 μm AFM image of this sample [Fig. 4(b)]. The four satellite peaks at diagonal directions indicate the high periodicity along the ⟨100⟩ direction in a wide area range. The alignment mechanism may be the same as the self-aligned SiGe island chain on Si (001) due to the strain field decaying monotonically along the elastically soft ⟨100⟩ direction.[30] Consequently, once the density of nanodots is high enough, the nanodots tend to align in this direction. Moreover, thanks to the vertical alignment, the lateral position of the nanodots is transferred to the next layer, thus improving the degree of order with increasing cycle number as can be seen in Fig. 3(a).

Figures 5(a)–5(b) show a high-angle annular dark field (HAADF) STEM image of the SL and an EDX line-scan profile of the marked area in Fig. 5(a). It is clear that the surface of $Si_{0.48}Ge_{0.52}$ deposited at 550 °C is flat, and the Ge nanodot grows on the buried nanodot. By contrast, the surface of $Si_{0.51}Ge_{0.49}$ deposited at 500 °C is rough, and the Ge nanodot tends to grow in the concave region. It is worth noticing that there are relatively white lines across the $Si_{0.51}Ge_{0.49}$ with one end near the bevel of the nanodot and the other end at the sidewall of the mesa [Fig. 5(a)]. These lines can be seen only in the $Si_{0.51}Ge_{0.49}$ deposited at 500 °C and they are Ge-rich according to the EDX line-scan as shown in Fig. 5(b). However, these white lines cannot be found above the center of the Ge nanodot, indicating uniform Ge concentration at the same region but 90° rotated position. Therefore, these Ge-rich lines are more likely two-dimensional planes than one-dimensional bars in the space.

To investigate the origin of the Ge-rich planes, 1.0 nm–1.5 nm Ge markers were introduced by pausing the SiH_4 flow 4 times during the SiGe spacer growth at 500 °C and 550 °C without changing the other process conditions as shown in Fig. 5(c). At 550 °C, the growth rate of $Si_{0.48}Ge_{0.52}$ on the wetting layer is larger than that on the Ge nanodot until the surface becomes smooth (see the third Ge marker in SiGe grown at 550 °C). By contrast, at 500 °C, the difference in $Si_{0.51}Ge_{0.49}$ growth rate on the wetting layer or on the Ge nanodot is less due to the insufficient surface migration of adsorbed Si and Ge atoms, retaining the rough SiGe surface.

In the case of 500 °C, with increasing thickness of SiGe, the mesa width increases, which is consistent with the AFM results as summarized in Fig. 2. Moreover, a stairstep feature can be seen on the SiGe mesa sidewall, and the Ge marker fills the bottom of each stairstep, forming a smooth Ge marker surface rather than stairs [Fig. 5(d)]. These may explain the formation of the Ge-rich planes in Fig. 5(a). The bottom corner of the stairstep is a more reactive and/or preferable location for Ge atom migration. Consequently, the

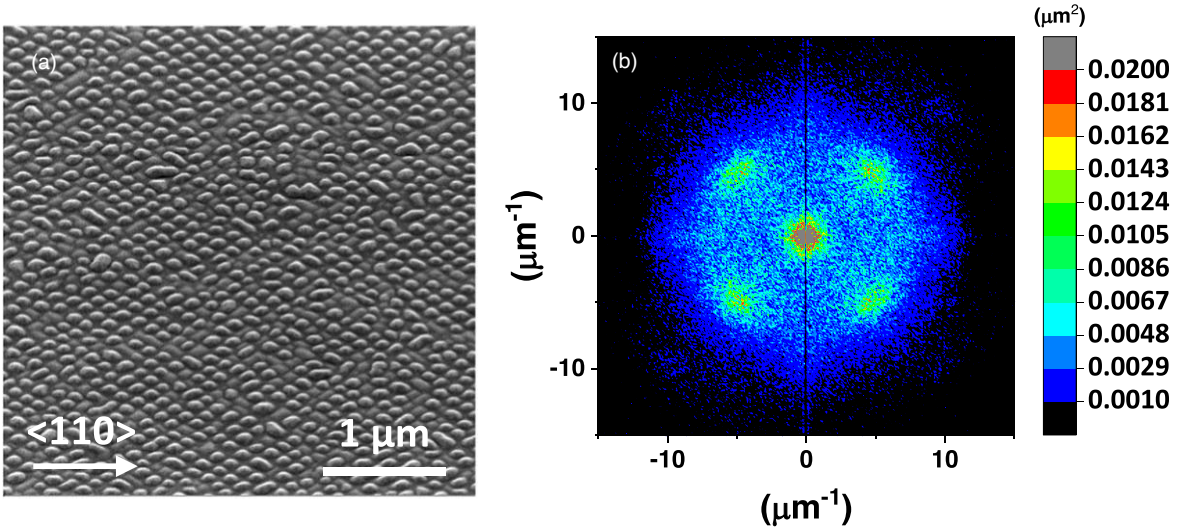

Fig. 4. (Color online) (a) Angle view of SEM image (view at an angle of 40° to the surface) and (b) FT image of a 10 μm × 10 μm AFM image of Ge nanodots on 20-cycle SL of 52 nm SiGe/12.5 nm Ge. $Si_{0.48}Ge_{0.52}$ grown at 550 °C and $Si_{0.51}Ge_{0.49}$ grown at 500 °C alternately used as spacers.

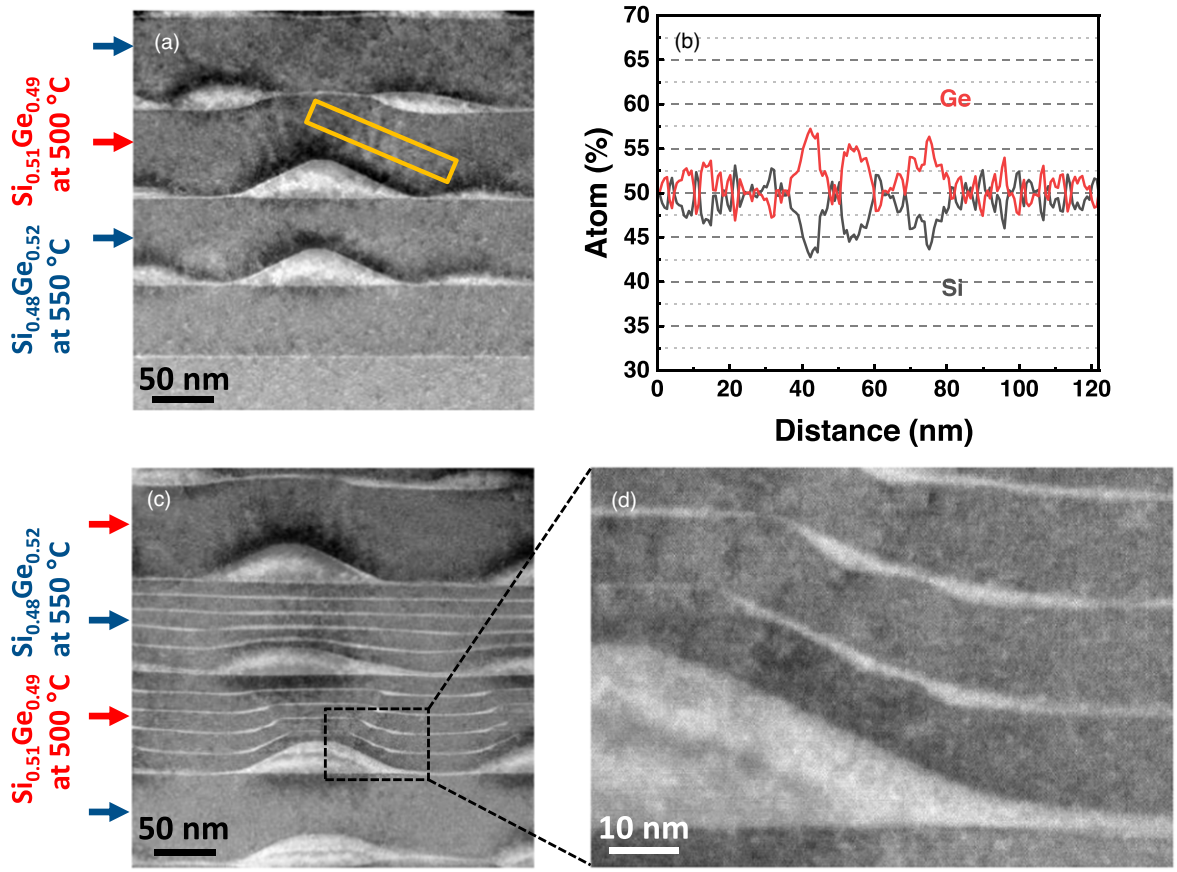

Fig. 5. (Color online) (a) HAADF STEM image of the same sample as shown in Fig. 3(a). (b) EDX line-scan of the region marked in orange color in the STEM image (a). (c) HAADF STEM image of the same SL with 1.0–1.5 nm Ge marker layers in the $Si_{0.51}Ge_{0.49}$ grown at 500 °C (marked with red arrows) and $Si_{0.48}Ge_{0.52}$ grown at 550 °C (marked with blue arrows). (d) Enlarged image of the marked region in (c).

bottom corner of the stairsteps becomes Ge-rich. During SiGe growth, these Ge-rich corner lines become tilt Ge-rich planes with increasing mesa width. In addition to the corner of the stairsteps, it seems the concave region between two dots is another preferable position for Ge growth. Ge marker layers are thicker in the concave region and thinner on top of the mesa as shown in Fig. 5(d), thus lowering the SiGe mesa height on the Ge nanodot and causing insufficient surface roughness for staggered alignment of Ge nanodot formation. As a result, the Ge nanodots no longer grow at the staggered positions on the $Si_{0.51}Ge_{0.49}$ grown at 500 °C after inserting the Ge marker layers.

To study the growth and alignment mechanism of Ge nanodots on the checkerboard mesa structured SiGe surface, the surface morphologies at different process steps are inspected. When the temperature is increased to the Ge growth temperature of 550 °C immediately before Ge deposition, the edge of the SiGe mesa is smoothed as shown in Fig. 6. In the early stage of Ge deposition [Fig. 7(a)], the mesa patterns look 45° rotated from the SiGe mesas in Fig. 1(c), implying nucleation of Ge nanodots starts on the sidewalls of the SiGe mesas. The same phenomenon is observed from the Ge marker in the $Si_{0.51}Ge_{0.49}$ grown at 500 °C in Figs. 5(c)–5(d). The bottom of the mesa sidewalls could be the preferable position to reduce the surface energy. With increasing Ge coverage, the Ge nanodots become higher and larger [Fig. 7(b)], and then merge with the vicinity dot in the same concavity [Figs. 7(c)–7(d)].

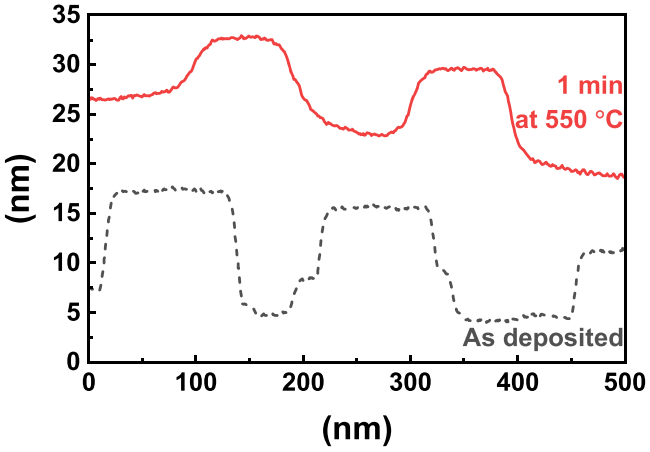

Fig. 6. (Color online) Line profiles of $Si_{51}Ge_{49}$ on laterally ordered Ge nanodot templates before and after holding at 550 °C for 1 min.

4. Summary and conclusions

3D-aligned Ge nanodots by SiGe/Ge SL deposition on SiGe VS were investigated. The surface morphology of the SiGe spacer changes by modifying the process condition. When the SiGe spacer is deposited at 500 °C on laterally aligned Ge nanodots along ⟨100⟩, a checkerboard mesa structure is formed on buried Ge nanodots. By increasing the deposition temperature or the Ge content, the SiGe surface becomes smoother due to enhanced surface migration. Ge nanodots tend to align dot-on-dot when the SiGe surface is smooth

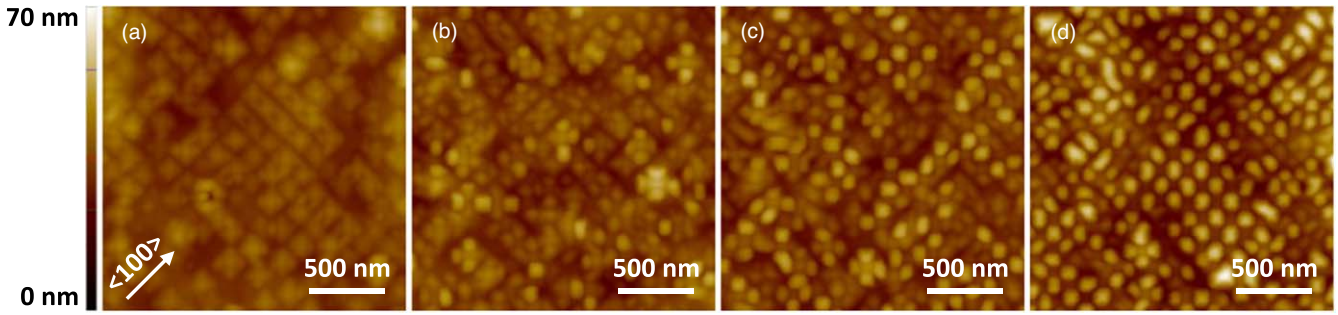

Fig. 7. (Color online) AFM images of 20-cycle SL of 52 nm SiGe/12.5 nm Ge. $Si_{0.48}Ge_{0.52}$ grown at 550 °C and $Si_{0.51}Ge_{0.49}$ grown at 500 °C alternately used as spacers, and top Ge coverage of (a) 2.5 nm, (b) 5.0 nm, (c) 7.5 nm and (d) 12.5 nm.

because of the local lateral tensile strain induced by the buried nanodots. However, when the SiGe surface is checkerboard mesa structured, Ge grows at the bottom of the mesa sidewalls first due to surface energy reduction, and then merges with others in the same concavity. As a result, the nanodots form at the staggered position (concavity) between two mesas. This enables the vertical alignment of multilayer Ge nanodots switching between dot-on-dot and staggered alignment. In addition to the vertical alignment, the Ge nanodots are laterally aligned along the elastically soft ⟨100⟩ direction without pre-structuring, which may result from the strain field distribution. Ge-rich planes found in the SiGe spacer grown at 500 °C are associated with more surface migration of Ge atoms compared to Si atoms and the preference of Ge growth at the bottom corner of stairsteps. The results obtained here enable alignment-controlled 3D-ordered Ge nanodot stacks.

Acknowledgments

The authors would like to thank the IHP cleanroom staff for technical support and processing wafers.

ORCID iDs

Wei-Chen Wen https://orcid.org/0000-0001-6804-9562
Yuji Yamamoto https://orcid.org/0000-0003-0928-4356

1) E. Kasper, Phys. Scr. **T35**, 232 (1991).
2) C. J. R. P. Augusto and L. Forester, Solid-State Electron. **110**, 1 (2015).
3) C. E. Pryor, M. E. Flatté, and J. Levy, Appl. Phys. Lett. **95**, 232103 (2009).
4) A. B. Talochkin, I. B. Chistokhin, and V. A. Markov, Nanotechnology **20**, 175401 (2009).
5) J. L. Liu, A. Khitun, K. L. Wang, T. Borca-Tasciuc, W. L. Liu, G. Chen, and D. P. Yu, J. Cryst. Growth **227-8**, 1111 (2001).
6) M. H. Liao, C.-Y. Yu, T.-H. Guo, C.-H. Lin, and C. W. Liu, IEEE Electron. Device Lett. **27**, 252 (2006).
7) K. L. Wang, J. L. Liu, and G. Jin, J. Cryst. Growth **237-9**, 1892 (2002).
8) M. Grydlik, F. Hackl, H. Groiss, M. Glaser, A. Halilovic, T. Fromherz, W. Jantsch, F. Schäffler, and M. Brehm, ACS Photon. **3**, 298 (2016).
9) P. Krause, J. C. Tremblay, and A. Bande, J. Phys. Chem. A **125**, 4793 (2021).
10) Q. Chen et al., ACS Appl. Nano Mater. **4**, 897 (2021).
11) S. Cosentino et al., Appl. Phys. Lett. **98**, 221107 (2011).
12) S. Shi, D. Pacifici, and A. Zaslavsky, Appl. Phys. Lett. **119**, 221108 (2021).
13) J. W. John, V. Dhyani, S. Singh, A. Jakhar, A. Sarkar, S. Das, and S. K. Ray, Nanotechnology **32**, 315205 (2021).
14) V. Le Thanh, V. Yam, Y. Zheng, and D. Bouchier, Thin Solid Films **380**, 2 (2000).
15) A. Alguno, N. Usami, T. Ujihara, K. Fujiwara, G. Sazaki, K. Nakajima, and Y. Shiraki, Appl. Phys. Lett. **83**, 1258 (2003).
16) P. S. Chen, Z. Pei, Y. H. Peng, S. W. Lee, and M. J. Tsai, Mater. Sci. Eng. B **108**, 213 (2004).
17) K. L. Wang, D. Cha, J. Liu, and C. Chen, Proc. IEEE **95**, 1866 (2007).
18) M. S. Storozhevykh, L. V. Arapkina, S. M. Novikov, V. S. Volkov, A. V. Arsenin, O. V. Uvarov, and V. A. Yuryev, J. Raman Spectrosc. **53**, 853 (2022).
19) Y. Yamamoto, P. Zaumseil, G. Capellini, M. Andreas Schubert, A. Hesse, M. Albani, R. Bergamaschini, F. Montalenti, T. Schroeder, and B. Tillack, Nanotechnology **28**, 485303 (2017).
20) Y. Yamamoto, Y. Itoh, P. Zaumseil, M. A. Schubert, G. Capellini, F. Montalenti, K. Washio, and B. Tillack, Semicond. Sci. Technol. **33**, 114014 (2018).
21) Y. Yamamoto, Y. Itoh, P. Zaumseil, M. A. Schubert, G. Capellini, K. Washio, and B. Tillack, ECS J. Solid State Sci. Technol. **8**, P190 (2019).
22) W. C. Wen, M. A. Schubert, M. H. Zöllner, B. Tillack, and Y. Yamamoto, ECS Trans. **109**, 343 (2022).
23) W.-C. Wen, B. Tillack, and Y. Yamamoto, Ext. Abstr. of the 2022 Int. Conf. on Solid State Devices and Materials (2022).
24) P. M. Mooney, Mater. Sci. Eng. R **17**, 105 (1996).
25) P. I. Gaiduk, A. N. Larsen, and J. L. Hansen, Thin Solid Films **367**, 120 (2000).
26) A. D. Capewell, T. J. Grasby, T. E. Whall, and E. H. C. Parker, Appl. Phys. Lett. **81**, 4775 (2002).
27) Y. Yamamoto, P. Zaumseil, T. Arguirov, M. Kittler, and B. Tillack, Solid-State Electron. **60**, 2 (2011).
28) Y. Yamamoto, P. Zaumseil, M. A. Schubert, and B. Tillack, Semicond. Sci. Technol. **33**, 124007 (2018).
29) G. Kissinger, T. Morgenstern, G. Morgenstern, and H. Richter, Appl. Phys. Lett. **66**, 2083 (1995).
30) M. Meixner, E. Schöll, M. Schmidbauer, H. Raidt, and R. Köhler, Phys. Rev. B **64**, 797 (2001).